Semiclassical maps: A study of classically forbidden transitions, sub-*h* structure, and dynamical localization

N. T. Maitra[a)]
Department of Chemistry, University of California at Berkeley, Berkeley, California 94720-1460

(Received 20 July 1999; accepted 13 October 1999)

Representing the dynamics of a continuous time molecular system by a symplectic discrete time map can much reduce the computational time. The question then arises of whether semiclassical methods can be effectively applied to this reduced description: as in the classical case, the map should prove to be a much more computationally efficient description of the dynamics. Here we study the semiclassical propagation of the standard map, or kicked rotor, based on a Herman–Kluk propagator. This is a very interesting playground to test the feasibility of a semiclassical mapping approach, since it demonstrates a wealth of quantum and classical dynamical behavior: As the kick strength increases, the system goes from being very nearly integrable, through mixed phase space, to chaotic. The map displays phenomena that occur in generic molecular systems, so this study is also a test of how well semiclassics can describe such phenomena. In particular, we discuss (i) classically forbidden transport: the significance of branches of the semiclassical integrand in the complex phase plane must be understood in order for the semiclassics to be meaningful; (ii) sub-*h* structure: in the nearly integrable regime, the semiclassics can be poor due to the presence of islets of area less than Planck's constant in phase space; (iii) dynamical localization: in the chaotic regime, the classical momentum diffuses, whereas the quantum localizes. Our results show that semiclassics also localizes, and we can confirm directly the theory that dynamical localization is due largely to phase interference. © *2000 American Institute of Physics.* [S0021-9606(00)31202-8]

I. INTRODUCTION

Maps have been used for many years to study the dynamics of nonlinear systems.[1–4] The most famous example is the Poincaré surface of section mapping,[1] which has proved to be very valuable in analyzing multidimensional systems: one can visualize the full global dynamics on a section of lower dimension. Also, the numerical computations are much faster, since part of the dynamics is effectively done analytically in obtaining the map itself. The idea of obtaining and exploiting a discrete-time map from a continous-time Hamilitonian system in chemical systems with multiple-time scales has been explored by a number of authors.[3] For example, for a system coupled to a bath, one could obtain an approximate map based on a time step long compared with the system vibrations but short on the relaxation time scale. In a recent paper,[4] it was shown how to obtain a kicked symplectic map based on perturbation theory from a continuous time Hamiltonian, where all the perturbations act instantaneously at the kick.

Given the many advantages of considering the discrete-time mapping approach to the continuous-time system, we are motivated to consider semiclassical propagation in such systems. As in the classical case, we would expect the discrete-time map requires much less numerical effort to reach the same physical time than its corresponding continous-time system, since part of the problem is done analytically.

Semiclassical methods have been a focus of interest since the birth of quantum mechanics,[5] and recently there has been a surge of interest in developing semiclassical techniques to describe complex molecular and chemical systems.[6] The essence of semiclassics is an approximate formulation of quantum mechanics in terms of only classical objects and Planck's constant. Stationary phase evaluation of Feynman's path integral for the quantum propagator results in the form $\Sigma\sqrt{\rho}e^{iS/\hbar}$, where the sum goes over all classical paths that link the two end points in the propagator. The phase S is the appropriate classical action for the path and the weighting ρ is a classical probability density together with any Maslov factors arising from caustics encountered by the path.[5] In practice, it is usually much more convenient to transform this to what is now often called an initial-value representation:[7,8] one trades in the boundary-value root search for the classical paths for an integral over all initial conditions. This has another advantage of being better behaved than the boundary-value propagator because the behavior near caustics can be uniformized. In this paper we present and study a uniformized semiclassical propagator for discrete-time kicked maps, based on a Herman–Kluk approach.

As a first test of the semiclassical map, in this paper we shall be studying the kicked rotor, or standard map. This is a one-dimensional map obtained from a two-degrees of freedom system through a Poincaré surface of section and has been studied in great depth[2] for two main reasons: (i) be-

a)Current address: Department of Chemistry, Rutgers, The State University of New Jersey, Piscataway, New Jersey 08854; electronic mail: nmaitra@neon.cchem.berkeley.edu

 © 2000 American Institute of Physics

Downloaded 06 Jun 2003 to 128.6.71.61. Redistribution subject to AIP license or copyright, see http://ojps.aip.org/jcpo/jcpcr.jsp

cause of its importance as a first-order approximation to a perturbation of an integrable system around a generic resonance, and (ii) because of the range of dynamical behavior (both classical and quantum) the map displays for different kick strengths. It is an approximate description of molecular behavior under periodic perturbations.[9] The classical map is close to integrable for very small kick strengths, islets of stability, and small zones of chaoticity separated by irrational KAM tori exist for slightly larger values of kick strength, global chaos begins to set in at the critical kick strength, where the last surviving KAM torus breaks into a cantorus, and for very large kick strength strong chaos reigns throughout phase space. This brings us to another motivation of this paper: in this yet one-dimensional problem lies a wealth of very interesting classical and quantum phenomena, which, moreover, occur in many-dimensional (continuous-time) molecular systems. In attempting to describe such complex quantum systems using semiclassics, one would like to have an idea whether such phenomena can, in principle and in practice, be reasonably described in this approximation. We will consider in particular, classically forbidden transport, the effect of classical islets of stability of area less than Planck's constant, and dynamical localization.

The essential property of interference in obtaining correct quantum amplitudes is built into the semiclassical approximation, and so this approximation describes interference well. A more contentious issue is the description of classically forbidden processes such as tunneling, and there has been a debate among several works in the literature[10–12] as to whether the real trajectories of the semiclassical propagator can describe behavior that explores regions of phase space untouched by the real trajectories. We shall encounter such a situation in Sec. III: after one iteration of the map, there is some quantum transport to states that are not reached by the classical distribution. Although this is somewhat different from the usual concept of tunneling through a barrier, it has the same essence of quantum transport into regions that are classically forbidden. The guiding classical trajectories for this behavior are indeed complex ones, and, in general, the branch structure in the complex plane prevents the real trajectories from picking up their contribution. A propagator in boundary-value representation, which explicitly includes complex trajectories, does a much better job. However, we show how we can push the branch cuts to infinity with a careful choice of an arbitrary parameter in the propagator in initial-value representation, and then the integral over real trajectories is equivalent to one deformed legally to include the relevant complex ones. Our conclusions here are similar to points discussed in recent work;[11,12] in contrast to those cases, we find here a case where we can almost exactly obtain the forbidden transition amplitudes from real trajectories in the procedure mentioned above.

Another interesting issue is how semiclassics copes when there is structure in phase space below the scale of Planck's constant h. h sets a lower limit on the area of classical phase space structures that quantum mechanics can resolve. The validity of the semiclassical approximation to Feynman's path integral hinges on the stationary phase contributions differing in action by more than h: otherwise the coalescence of such stationary phase paths makes the simple sum over classical paths mathematically incorrect. The classical dynamics on which semiclassics is based, and the quantum dynamics, are very different. In Sec. IV we explore the situation where the phase space is very nearly integrable but containing islets of area less than h, and find indeed that these islets cause the semiclassical approximation to be worse. This is somewhat related to the blow-up of semiclassics near caustics; however, unlike that case, there is no representation for which the problem of the presence of sub-h islets can be uniformized.

Of great interest is the phenomenon of dynamical localization:[13] in many classically chaotic systems where there is slow diffusion in one variable (slow compared with the time scales of the other variables), the quantum dynamics shows, in dramatic contrast, localization in that variable. In fact, the kicked rotor is the paradigm of this effect, although dynamical localization, of course, occurs in real molecular systems, for example, for systems driven by a laser field, or some other periodic perturbation.[9] The quantum behavior follows the classical until the ''break time,'' or quantization time, which is the time required to resolve all the eigenstates in the wave packet (i.e., the inverse level spacing). After this time, the quantum dynamics becomes quasiperiodic, and the diffusion shuts down. The effect can be understood from considering when interference effects begin to become significant, so we expect that semiclassics should be able to describe dynamical localization. This has been hard to show explicitly because of the exponential proliferation of necessary trajectories that chaos brings into the semiclassical calculation. There has so far been one study of this,[14] where semiclassical localization is shown for a particularly designed caustic-free map, implementing an essentially exact iterated approximation to the semiclassical propagator in boundary-value representation. Here in Sec. V we attempt to demonstrate semiclassical dynamical localization directly using a semiclassical propagator in an initial-value representation for the archetypal kicked rotor and to show that it is due to interference between the classical terms composing the semiclassical propagator. We can propagate to times long enough to see the localization setting in, but have not propagated for much longer because the calculation takes exponentially long.

One iteration of the standard map transforms the canonically conjugate variables on a cylinder (θ,I) to (θ',I'), where

$$I' = I + k \sin\theta, \quad \theta' = \theta + I' \pmod{2\pi}. \tag{1.1}$$

Typical phase spaces for the system at various kick strengths are shown in Fig. 1.

One may associate a time-dependent Hamiltonian with the map $H = I^2/2 + k\cos(\theta)\Sigma_n \delta(t-n)$. However, this is not a unique choice: for any $0 < \eta < 1$, a Hamiltonian whose potential term acts first for a fraction η of the period and the kinetic term for the rest of the period also effects the equations of motion above:

Downloaded 06 Jun 2003 to 128.6.71.61. Redistribution subject to AIP license or copyright, see http://ojps.aip.org/jcpo/jcpcr.jsp

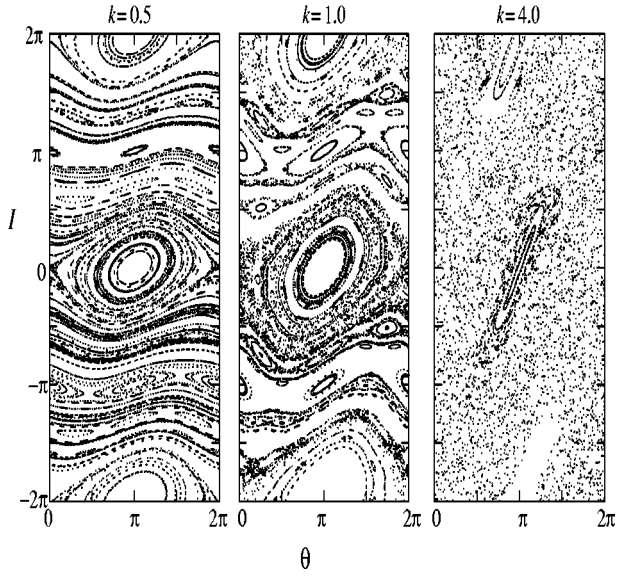

FIG. 1. Phase spaces for the kicked rotor: as k increases so does the degree of chaos, and the sizes of the islets of stability shrink.

$$H=\frac{1}{\eta}k\cos\theta, \quad 0<\tau<\eta$$
$$=\frac{I^2}{2(1-\eta)}, \quad \eta<\tau<1, \tag{1.2}$$

where $0\leqslant\tau\leqslant 1$ measures the ''time'' within the period.

II. SEMICLASSICAL PROPAGATION FOR MAPS

The semiclassical propagator for n iterations of a symplectic kicked map is given by[1,5]

$$\langle\theta_f|U^n|\theta_i\rangle=\sum_{\rm cl}\sqrt{\frac{-1}{2\pi i\hbar}\frac{\partial^2 F_1^n}{\partial\theta_i\,\partial\theta_f}}\,e^{iF_1^n(\theta_f,\theta_i)/\hbar-i\pi\nu/2}, \tag{2.1}$$

where F_1^n is the type-1 generating function[15] for n iterations of the map. The sum goes over all classical trajectories that map θ_i to θ_f in n iterations. F_1^n plays the role that the action does in the continuous-time case, generating the canonical transformation for the map: the initial and final momenta I_i and I_f are $I_i=-\partial F_1^n/\partial\theta_i$, $I_f=\partial F_1^n/\partial\theta_f$. Just as in the continuous-time case, the prefactor weighs the classical trajectory according to the classical probability, and ν is the Maslov index, counting the number of caustics encountered by the trajectory.

The semiclassical propagator has the same form in all representations, with the appropriate change in the generating function, as was shown in the ''semiclassical algebra'' of Miller's.[5] For example, to compute $\langle I_f|U|I_i\rangle$, the type-1 generating function is replaced by the type-4 generating function $F_4(I_f,I_i)=F_1(\theta_f,\theta_i)+\theta_i I_i-\theta_f I_f$. We shall refer to semiclassical propagators of the form (2.1) as boundary-value Van-Vleck (or BVV) propagators.

Although it is simple to compute the classical trajectories and hence the propagator for one step of the map, it becomes much harder to solve the boundary-value problem for more than one-step and the number of contributing classical trajectories grows exponentially as time evolves for a chaotic map (large k for the kicked rotor). Instead, we transform to an initial-value representation for the propagator,[7,8] where we integrate over the phase space of initial conditions for the trajectories. Moreover, we use a representation in which there are no caustics (in the real phase plane). This is the coherent state representation, whose use in semiclassical methods was introduced by Heller.[16] Heller's expansion in ''frozen Gaussians'' was further developed to give various forms of semiclassics in coherent state representation, perhaps the most well known of which is the Herman–Kluk propagator.[8] In our study we use a Herman–Kluk type of propagator appropriate to our cylindrical phase space, and we now discuss this.

The Herman–Kluk propagator in Cartesian variables in one dimension gives[8]

$$\langle\psi_f|U(t)|\psi_i\rangle=\int\frac{dq_0\,dp_0}{2\pi\hbar}\langle\psi_f|q_t,p_t\rangle \times C_{q_0p_0t}e^{iS(q_0,p_0,t)/\hbar}\langle q_0,p_0|\psi_i\rangle. \tag{2.2}$$

This was derived[8] by inserting the identity in the form of the (over-)completeness relation in coherent states several times in the expression involving (the continuous time version of) Eq. (2.1) and then performing integrals by the stationary phase. It has also been shown to result from performing the stationary phase directly on Feynman's path integral in the coherent state representation.[17] The coherent states $|q_c,p_c\rangle$ are defined by

$$\langle q|q_c,p_c\rangle=\left(\frac{2\gamma}{\pi}\right)^{1/4}e^{-\gamma(q-q_c)^2+ip_c(q-q_c)/\hbar}, \tag{2.3}$$

γ is the width parameter for the coherent state, which we are free to choose: $\sigma_q=\sqrt{\langle\Delta q^2\rangle}=1/(2\sqrt{\gamma})$ and $\sigma_p=\sqrt{\langle\Delta p^2\rangle}=\hbar\sqrt{\gamma}$. (q_0,p_0) are initial conditions for the trajectory, which evolves under Hamilton's equations to (q_t,p_t) in time t and $S(q_0,p_0,t)=S[q_t(q_0,p_0),q_0,t]$ is the classical action along the path. The prefactor

$$C_{q_0p_0t}=\sqrt{\frac{1}{2}\left(\frac{\partial q_t}{\partial q_0}+\frac{\partial p_t}{\partial p_0}-2i\hbar\gamma\frac{\partial q_t}{\partial p_0}-\frac{1}{2i\hbar\gamma}\frac{\partial p_t}{\partial q_0}\right)}$$

involves elements of the stability matrix, which, in contrast to the boundary-value formulation, are in the numerator rather than the denominator. Many interesting issues and problems arise when implementing this prescription for the semiclassical propagator, in particular, (i) convergence problems for chaotic systems where the integrand grows exponentially with time and becomes highly oscillatory; (ii) how, and whether these real trajectories can describe classically forbidden processes, which are, by contrast, associated with complex classical paths. We shall encounter such issues when studying our discrete-time map, so we will defer until then a broader discussion of this propagator.

We now describe how we adopt a Herman–Kluk type of propagator for discrete-time maps on a cylinder. We require that any allowed wave functions respect the following continuity condition in an angle:

$$\psi(\theta+2\pi m)=\psi(\theta), \text{ for an m integer.} \tag{2.4}$$

This requirement imposes a quantization condition on the canonically conjugate variable, I:

Downloaded 06 Jun 2003 to 128.6.71.61. Redistribution subject to AIP license or copyright, see http://ojps.aip.org/jcpo/jcpcr.jsp

$$\langle\theta|I\rangle=\frac{1}{\sqrt{2\pi}}e^{iI\theta/\hbar}\ \text{exists only if}\ I=j\hbar, \tag{2.5}$$

where j is an integer. Completeness relations in angle and action states are $\Sigma_j|I_j\rangle\langle I_j|=\mathbf{1}$, where $I_j=j\hbar$ and $\int_0^{2\pi}|\theta\rangle\langle\theta|d\theta=\mathbf{1}$. The correctly periodized coherent states centered at (θ_c,I_c) on the cylinder have angle representation,

$$\langle\theta|\theta_c,I_c\rangle=\sum_m\langle\theta|\theta_c+2\pi m,I_c\rangle_\infty, \tag{2.6}$$

$$=\left(\frac{2\gamma}{\pi}\right)^{1/4}\sum_m e^{-\gamma(\theta-\theta_c-2\pi m)^2+iI_c(\theta-\theta_c-2\pi m)/\hbar}, \tag{2.7}$$

where $\langle\theta|\theta_c,I_c\rangle_\infty$ indicates the usual infinite-space coherent state. In action representation, they have the form

$$\langle I|\theta_c,I_c\rangle=\int_0^{2\pi}d\theta\langle I|\theta\rangle\langle\theta|\theta_c,I_c\rangle$$

$$=\left(\frac{1}{2\pi\gamma}\right)^{1/4}e^{-(I-I_c)^2/(4\hbar^2\gamma)-iI\theta_c/\hbar}, \tag{2.8}$$

which are defined only for $I=j\hbar$ with j an integer, but the center momentum of the coherent state I_c can be any real number. These coherent states satisfy the (over)-completeness relation

$$\frac{1}{2\pi\hbar}\int_0^{2\pi}d\theta\int_{-\infty}^{\infty}dI|\theta,I\rangle\langle\theta,I|=\mathbf{1}, \tag{2.9}$$

which is a crucial property in transforming Eq. (2.1) to an initial-value representation of the Herman–Kluk form. In the same way that the Herman–Kluk propagator was derived for continuous-time systems on an infinite phase space, we insert the identity in the form of our completeness relations (2.9). Although our integrals in angle in the completeness relations are only over $[0,2\pi)$, the sums in (2.7) can be used to transform the integrals to over $(-\infty,\infty)$, making the analysis identical to that in the infinite phase-space case.[8] We thus arrive at a Herman–Kluk type of propagator for a discrete-time map on a cylinder:

$$\langle\psi_f|U^n|\psi_i\rangle=\frac{1}{2\pi\hbar}\int_0^{2\pi}d\theta_0\int_{-\infty}^{\infty}dI_0\langle\psi_f|\theta_n,I_n\rangle$$

$$\times C_{\theta_0,I_0,n}e^{iF(\theta_0,I_0,n)/\hbar}\langle\theta_0,I_0|\psi_i\rangle, \tag{2.10}$$

where (θ_0,I_0) are the initial conditions for a trajectory that maps to (θ_n,I_n) after n iterations. The coherent states are defined as in Eqs. (2.7) and (2.8). The role of the action is played by $F(\theta_0,I_0,n)=F_1^n(\theta_n(\theta_0,I_0),\theta_0,n)$, where, as before, F_1^n is the type-1 generating function for n iterations, and may be composed as

$$F(\theta_0,I_0,n)=\sum_{p=0}^{n}F_1^1[\theta_{p+1}(\theta_p,I_p),\theta_p]. \tag{2.11}$$

For the kicked rotor (1.1),

$$F_1^1(\theta_{p+1}(\theta_p,I_p),\theta_p)=\tfrac{1}{2}(I_p+k\sin\theta_p)^2-k\cos\theta_p. \tag{2.12}$$

The prefactor is

$$C_{\theta_0,I_0n}=\sqrt{\frac{1}{2}\left(\frac{\partial\theta_n}{\partial\theta_0}+\frac{\partial I_n}{\partial I_0}-2i\hbar\gamma\frac{\partial\theta_n}{\partial I_0}-\frac{1}{2i\hbar\gamma}\frac{\partial I_n}{\partial\theta_0}\right)}, \tag{2.13}$$

where we may obtain the monodromy matrix elements by a simple matrix multiply at each iteration:

$$\begin{pmatrix}\frac{d\theta_n}{d\theta_0}&\frac{d\theta_n}{dI_0}\\ \frac{dI_n}{d\theta_0}&\frac{dI_n}{dI_0}\end{pmatrix}=\begin{pmatrix}1+k\cos\theta_{n-1}&1\\ k\cos\theta_{n-1}&1\end{pmatrix}$$

$$\times\begin{pmatrix}\frac{d\theta_{n-1}}{d\theta_0}&\frac{d\theta_{n-1}}{dI_0}\\ \frac{dI_{n-1}}{d\theta_0}&\frac{dI_{n-1}}{dI_0}\end{pmatrix}, \tag{2.14}$$

where the first matrix on the right contains the one-step monodromy matrix elements, $d\theta_n/d\theta_{n-1}$, etc.

Although there are no caustics in this representation, there is the (different) issue of a consistent choice of branch for the square root. The square root $\sqrt{z}$ is a double-valued function on the complex plane; numerical definitions choose the positive root on the positive real line with a branch cut along the negative real line. Discontinuities arise if z passes across the negative real axis. In the continuous-time case, the correct choice of branch can be obtained by requiring the square root to be continuous in time. There is no reason, however, for the integrand, nor the branch in the prefactor, to vary in a smooth way from one kick to the next in a discrete-time map. If we considered the evolution within each time step as dictated by integrating Hamilton's equations for a Hamiltonian of the form (1.2), then we effectively revert to the continuous-time case, and the branch choice would be continuous as a function of the integration time step (provided, as usual, that the integration time step is small enough). But if we need to numerically track the prefactor and sign changes with these much smaller time steps, then we lose the numerical advantage that the map provides, as discussed in the Introduction, and so one of the main points of this paper is defeated. In fact, the form of Hamiltonian (1.2) redeems us: we are able to analytically track the correct branch of the square root through the time step in the following way. During the first fraction of the period where the Hamiltonian is purely potential, the angle and its first derivatives remain at their value at the beginning of the period. Moreover, the momentum and its first derivatives change linearly in the time τ. This means that $C^2_{\theta_0,I_0,n+\tau}$ evolves from its $\tau=0$ value in the complex plane along a straight line. One can then simply check if this line crosses the negative real axis in order to determine whether a phase correction to the numerical computation is necessary. This simple process also holds for the second stage of the evolution within the period, where the Hamiltonian is purely kinetic; the discussion above holds with the roles of momentum and angle reversed. This is a very quick process for each time step.

Downloaded 06 Jun 2003 to 128.6.71.61. Redistribution subject to AIP license or copyright, see http://ojps.aip.org/jcpo/jcpcr.jsp

In all our studies we consider transport between momentum states: $|\psi_f\rangle=|I_f\rangle, |\psi_i\rangle=|I_i\rangle$, since this representation turns out to provide the most interesting phenomena. The momenta I_f and I_i have values of integer$\times\hbar$.

We compare our results with the fully quantum propagator, which we obtain in the following way. For one step, the unitary time evolution operator is

$$U^1_{qm}=e^{-iI^2/(2\hbar)}e^{-ik\cos\theta/\hbar}, \tag{2.15}$$

where I, θ are understood to be operators in this equation. This has the matrix elements

$$\langle I_f|U^1_{qm}|I_i\rangle=\frac{e^{-iI_f^2/(2\hbar)}}{2\pi}\int_0^{2\pi}d\theta\, e^{i(\theta_f-\theta_i)/\hbar}e^{-ik\cos\theta}. \tag{2.16}$$

We could obtain the matrix element after n iterations by matrix multiply, however, it is much faster to do a forward and backward fast Fourier transform as follows:[13]

$$\begin{aligned}\langle I_f|U^n_{qm}|I_i\rangle&=\sum_j\langle I_f|U^1_{qm}|I_j\rangle\langle I_j|U^{n-1}_{qm}|I_i\rangle\\&=\frac{e^{-i(I_f^2/2\hbar)}}{2\pi}\sum_p e^{-i(2\pi pf/N)}e^{-ik\cos(2\pi p/N)}\\&\quad\times\sum_j e^{i(2\pi pj/N)}\langle I_j|U^{n-1}_{qm}|I_i\rangle,\end{aligned} \tag{2.17}$$

where $I_f=f\hbar$ and N is the dimension of the Fourier transform, which we determine by the number of momentum states that are likely to be reached in the evolution.

III. ONE ITERATION AND CLASSICALLY FORBIDDEN TRANSPORT

We begin our study of the discrete-time map semiclassical propagator (2.10) by considering one iteration of the map. We shall show that our propagator provides a very good approximation for classically allowed transitions. The propagator is not, in general, able to describe well the transitions to classically forbidden states. We show why and how this problem can be overcome. We point out that these problems arise in generic semiclassical methods and our conclusions here hold for general systems and semiclassical propagators.

First, let us consider the classical evolution. We shall take the kick strength $k=10$ in this section, for definiteness, although the essential conclusions are similar for all k. For any k, in one iteration the line of initial conditions at I_i becomes curved as a sheared sine function, where the amplitude and degree of shearing depends on k. In the inset in Fig. 2 we have plotted this for $k=10$ for an initial manifold at $I_i=0$. The limits of the classical once-iterated distribution are at $|I_f-I_i|=k$. The main plot shows the square root of the (classical) probability of the trajectory reaching momentum I_f after one iteration, $\sqrt{P(I_f,I_i)}$. This is measured by counting the number with an end point in a bin of width 1, centered around I_f. We have chosen the bin size to coincide with the value of $\hbar=1$ that we shall use in the quantum and semiclassical calculations. Notice how the probability grows as the ''turning point'' at $|I_f-I_i|=k$ is approached: this is similar to the more familiar growth of the classical probability in position space at the turning points in a potential well.

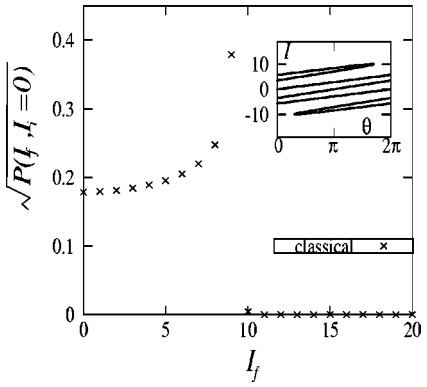

FIG. 2. The square root of the classical probability $\sqrt{P(I_f,I_i=0)}$, as described in the text. The inset shows the classically evolved manifold in phase space.

The magnitude of the quantum distribution, calculated through Eq. (2.17) for $n=1$, is plotted as $*$ connected by the dashed line in Fig. 3. Of course, the probability does not exist at points between the stars; we have just connected them for ease of visualization. Notice how this oscillates around its classical analog in Fig. 2, due to interference. Notice also the tail of the distribution beyond $|I_f-I_i|=k=10$; this classically forbidden transport resembles the tunneling tails of wave functions into classically forbidden regions into a barrier, for example. The other plots in this figure are from semiclassical calculations. All except that labeled ''bvv'' are computed from Eq. (2.10) and their label indicates the width parameter γ of the coherent state taken in the frozen Gaussian expansion. We are free to choose γ in

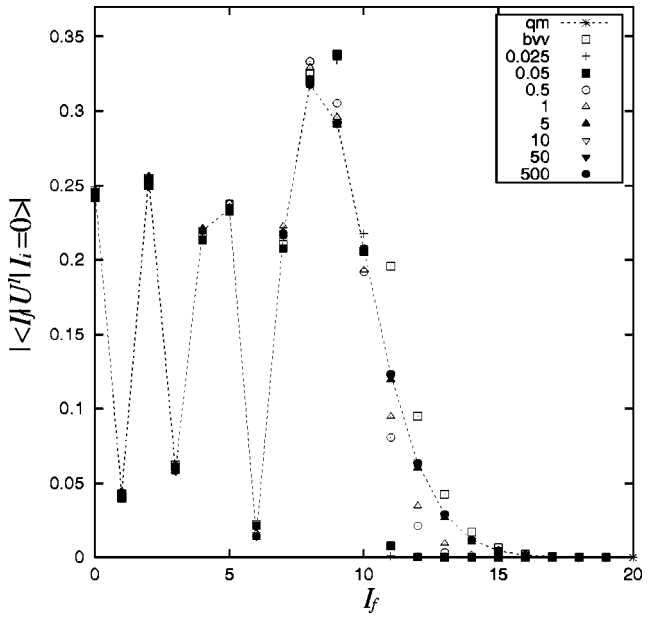

FIG. 3. The probability amplitude $|\langle I_f|U^1|I_i=0\rangle|$, for $k=10$, computed ($-*-$) quantum mechanically [Eq. (2.17)], and semiclassically [Eq. (2.10)], with the value of γ as indicated in the key. The Van-Vleck propagator (bvv) (3.3), analytically continued to complex trajectories is shown as the open square.

Downloaded 06 Jun 2003 to 128.6.71.61. Redistribution subject to AIP license or copyright, see http://ojps.aip.org/jcpo/jcpcr.jsp

Eq. (2.10): it determines the representation that the actual semiclassics is being performed in (e.g., $\gamma=0.5$ means that the semiclassical approximation is done in round coherent states, with equal uncertainty in I and θ). There is practically exact agreement for all the semiclassical calculations with the quantum distribution for final actions in the classically allowed region. However, for most γ, the semiclassical propagator does not capture the classically forbidden behavior well at all; yet for others it is almost exact.

The reason why the integral of (2.10) is, in general, poor in describing the classically forbidden transport lies in its failure to access the complex trajectories that would dominate the full quantum path integral: these are the stationary paths of the quantum path integral for the classically forbidden process. The integral (2.10) is over only real trajectories and is not, in general, deformable to, nor therefore the same as, an integral passing through the complex stationary phase points: they are hidden behind a branch cut in the complex phase plane emanating from the zeros of the prefactor $C_{\theta_0,I_0,1}$. This point was also raised recently,[11] where tunneling across the Eckart barrier was considered in an initial-value representation.

The position of the branch cut depends on the frozen Gaussian width γ: the prefactor for one iteration is

$$C_{\theta_0,I_0,1}=\sqrt{1-i\hbar\gamma+\frac{k\cos\theta_0}{2}\left(1-\frac{1}{2i\hbar\gamma}\right)}, \tag{3.1}$$

which has a branch cut when

$$\cos\theta_0|_{\rm cut}=\frac{4i\hbar\gamma(1-i\hbar\gamma)}{k(2i\hbar\gamma-1)}. \tag{3.2}$$

For very small γ (momentum-state-like Gaussians) this gives $\theta_0|_{\rm cut}=\pi/2+i\epsilon$, where ϵ is very small, which is very close to the real-θ axis. But for large γ (angle-state-like Gaussians), $\theta_0|_{\rm cut}=\pi/2+i/\epsilon$, which is very far from the real axis. Now, the complex stationary phase path that guides the classically forbidden transport is determined by where the classical ''action'' $F(\theta_0,I_0,1)$ is stationary and does not depend on γ. For one iteration, this path has initial angle $\sin\theta_0=I_f/k$, where I_f is the final momentum in question. This means that γ determines the degree to which the stationary phase point is hidden behind the branch cut, and therefore the effectiveness of the real-phase-space integral in capturing the classically forbidden process. In particular, we expect for our problem that for very large γ the classically forbidden transport is captured very well, since the branch cuts retreat to infinity. Indeed in Fig. 3, as we turn γ up from very small, the probabilities in the classically forbidden region get better and better until a certain γ, at which they match almost exactly onto the quantum probabilities and beyond which they do not change. This is consistent with our analysis above with the limiting γ being the one at which the branch cut has passed above the stationary phase point in the complex plane and so no longer prevents the deformation of the real-θ_0 contour to pass through the stationary phase point. Notice there is very little difference in the classically allowed region: the choice of γ is truly arbitrary here. This is because the stationary paths here are all real so the branch cut in the complex plane does not affect the integral at all, i.e., the integration contour over the real trajectories is identical to the contour through the stationary phase trajectories. There is some disparity near the momentum caustic, we shall come back to this point shortly.

We can show explicitly that the classically forbidden transitions are due to complex classical trajectories by considering the boundary-value Van-Vleck propagator in momentum states. This is almost equivalent to the $\gamma\to 0$ limit of the initial-value formulation (2.10): the difference is that it includes complex classical trajectories when the expression is analytically continued. This kind of idea was introduced into chemical physics in the 1970s,[18] where atom–diatom collisions were discussed: classically forbidden transition amplitudes were obtained from analytically continued classical trajectories. The BVV momentum–momentum propagator is

$$\begin{aligned}\langle I_f|U^1|I_i\rangle&=\sum_{\rm cl}\sqrt{\frac{-1}{2\pi i\hbar}\frac{\partial^2F_4}{\partial I_i\partial I_f}}e^{iF_4(I_f,I_i)/\hbar}\\&=\sqrt{\frac{-1}{2\pi i\hbar k\sqrt{1-\left(\frac{I_f-I_i}{k}\right)^2}}}\\&\quad\times e^{-i/\hbar(I_f^2/2+(I_f-I_i)\arcsin[I_f-I_i/k])}\\&\quad\times(e^{-ik/\hbar\sqrt{1-[I_f-I_i/k]^2}}-ie^{ik/\hbar\sqrt{1-[I_f-I_i/k]^2}}),\end{aligned} \tag{3.3}$$

where $\theta_i=\partial F_4/\partial I_i$, $\theta_f=-\partial F_4/\partial I_f$. Graphically, this arises from the intersections in phase space of a line at I_f with the manifold obtained by one iteration of the map performed on a line at I_i. From the inset in Fig. 2, we see there are two intersections for $|I_f-I_i|<k$, a tangency at the caustics at $I_f-I_i=\pm k$, and no intersections otherwise (since $\pm k$ is the limit that the classical distribution in momentum can reach in one iteration of the map). We can, however, extend the BVV (3.3) to the classically forbidden region beyond $I_f-I_i=\pm k$ by analytically continuing (3.3) to these momenta; this is equivalent to including the complex trajectories, which would give the stationary phase contribution to the path integral from which (3.3) was derived. The result is plotted in Fig. 3 as the open boxes. There is mostly excellent agreement with the quantum [and the initial-value semiclassics equation (2.10)] in the classically allowed region, and the BVV captures reasonably well the tunneling into the classically forbidden region, overestimating it somewhat. The BVV fails around the caustic, and blows up to infinity right at the caustic. We shall comment on this at the end of this section.

Similar conclusions regarding integrals over real trajectories and tunneling have been made.[11,12] That the initial-value representation for tunneling is only accurate when the integration contour over real trajectories is deformable to a contour of steepest descent in the complex plane has been pointed out earlier.[11] There, tunneling across an Eckart barrier is considered, and it is shown that the integral in the

Downloaded 06 Jun 2003 to 128.6.71.61. Redistribution subject to AIP license or copyright, see http://ojps.aip.org/jcpo/jcpcr.jsp

initial-value representation is equivalent to a combination of integrals through both the steepest descent paths through roots and through caustics, rather than just through the roots. A complex (and time-dependent) value of γ is considered there to try to minimize the effects of caustics.

The significance of branch structure in the complex plane for classically forbidden processes was pointed out in recent work,[12] although in a different context. Tunneling through a barrier and above-barrier reflection in the time and energy domains was studied there. The exact numerical Fourier transform of time domain BVV semiclassics to the energy domain was considered and compared with a direct energy domain WKB formula. The WKB formula is equivalent to a stationary phase evaluation of the time domain semiclassics, including complex stationary paths, and does a much more accurate job than the exact numerical Fourier transform, which contains only real paths. This is because the integration contour through stationary phase points is distinct from the real-time integration axis because of a branch cut in the complex-time plane. It was found that if the position of the initial wave packet in the asymptotic region of the potential is brought closer to the barrier, the numerical FT improved, although this is a nonphysical effect, since probability amplitudes should not change when in the asymptotic region. This was attributed to the stationary phase point coming out of hiding behind the branch cut to a certain degree as the initial wave packet is moved in, and so a legal deformation of the real-time integral can pick up some of its contribution. This is very similar to the situation described in this section. Here, the analog of the energy domain WKB is the BVV propagator and that of the exact numerical Fourier transform is the integral over real initial conditions in the initial-value propagator. The parameter γ has an analogous effect to the wavepacket's initial position. However, it is of vital importance to realize that there is a major difference in that the barrier tunneling time-to-energy results should for physical reasons be independent of the initial position in the asymptotic region, whereas in the current situation involving the initial-value propagator, the parameter γ is ours to choose. In other words, in the barrier tunneling time-to-energy problem the branch cuts are set by the physical parameters in the problem, and there is no ''arbitrary'' parameter that we are at liberty to choose in an attempt to push the branch cuts to infinity. In fact, it is the time-domain semiclassics that is missing a tunneling contribution:[12] when this correction is added, the real-time integral to the energy domain is redeemed.

We conclude this section with a discussion about the behavior around the momentum caustics. Recall that the BVV above was poor in describing transitions to states that are a distance $\hbar$ away from the caustic, and it blows up to infinity at the caustic. If we use a noninteger value of k with an integer value of $\hbar$, then the BVV prefactor remains always finite, but for the momentum states that are within $\hbar$ of k, the BVV is still poor. For these states, the two contributions to the BVV (3.3) enclose a fold whose area in phase space is smaller than $h/2$ and this is what causes the BVV to fail: The stationary phase evaluation of the full path integral, which results in the semiclassical BVV, depends on the classical contributions (stationary points) being well separated in phase space compared to Planck's constant h. For γ not too small, the initial-value propagator (2.10) does not have this problem: the semiclassical approximation of Eq. (2.10) is in a coherent state representation in which there are no caustics on or near the real phase plane. The integral in Eq. (2.10) to go from coherent states to the initial and final momentum states is done numerically exactly, rather than by the stationary phase, and so is not equivalent to the BVV in momentum representation: it is uniformized. It is not surprising that as the coherent state representation in (2.10) is made more and more momentumlike (small γ), the approximation becomes worse near the caustic.

The effect of such a ''sub-h'' structure in phase space is discussed more in the next section, where we encounter different examples of more severe consequences: there, semiclassics for any γ is poor.

IV. NEAR-INTEGRABLE REGIME: PHASE-SPACE AREAS BELOW PLANCK'S CONSTANT

Above, we saw that a careful choice of the gaussian width parameter in Eq. (2.10) can overcome the problems caused by phase-space structure of area less than $h/2$ near a caustic. In this section, however, we discuss situations where the ''sub-h'' problem of semiclassics cannot be conquered. Again, this is a phenomenon that occurs in generic systems, in continuous-time systems and infinite phase spaces also, so our conclusions here should hold generally.

It is often assumed that semiclassics works well in integrable or nearly-integrable systems: in fact, this is not always true due to sub-h structure in phase space. The nearly integrable limit of our map is small k (see Fig. 1), where most of the invariant tori persist and some break up into small islets with very thin zones of chaoticity around the separatrices (hardly visible in our pictures at very small k). For very small k, the quantum mechanics is hardly perturbed from the integrable $k=0$ case, and there is very little transport in momentum. Yet, for this simple dynamics the semiclassics fails! In Fig. 4, we have plotted for $k=0.01$ and an initial momentum $I_i=0$, the semiclassical norm as a function of time computed from Eq. (2.10) using $\gamma=0.5$ and $\gamma=0.05$: in both cases, the drop down from 1 indicates the poorness of the approximation. We define Δ as the following expectation value of the difference of the semiclassical and quantum evolution operators:

$$\Delta=\langle I_i|(U_{qm}-U_{sc})(U_{qm}-U_{sc})^{\dagger}|I_i\rangle$$
$$=\sum_j |\langle I_j|U_{qm}-U_{sc}|I_i\rangle|^2, \tag{4.1}$$

which, for $k=0.01$, is plotted as a function of time in the lower half of Fig. 4. We have plotted this using both the unnormalized semiclassics as well as the renormalized semiclassics (where the amplitudes are renormalized to sum to 1). In Fig. 5, we plot at certain times the magnitude of the (unnormalized) wave function for $\gamma=0.5$ and $\gamma=0.05$.

Downloaded 06 Jun 2003 to 128.6.71.61. Redistribution subject to AIP license or copyright, see http://ojps.aip.org/jcpo/jcpcr.jsp

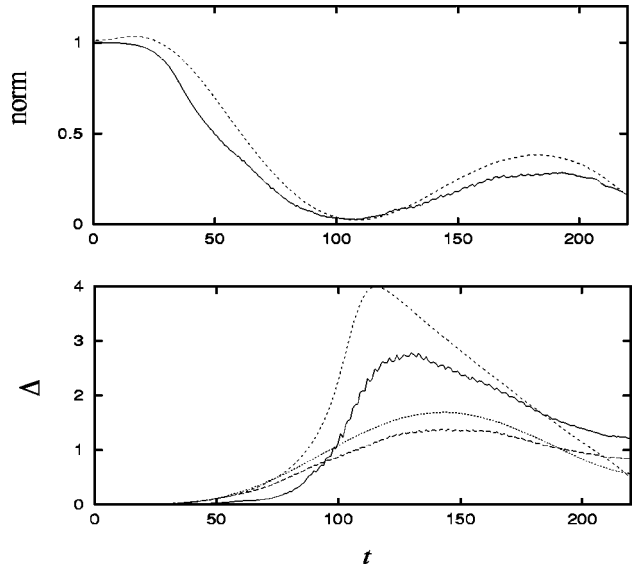

FIG. 4. The upper figure shows the norm of the semiclassical wave function for $k=0.01$ as a function of time, γ is equal to 0.5 (solid line) and 0.05 (dashed line). The lower figure plots Δ (see the text): $\gamma=0.5$, renormalized semiclassics (solid line), $\gamma=0.5$, unnormalized (long-dashed line), $\gamma=0.05$, renormalized semiclassics (short-dashed line), $\gamma=0.05$, unnormalized (dotted line).

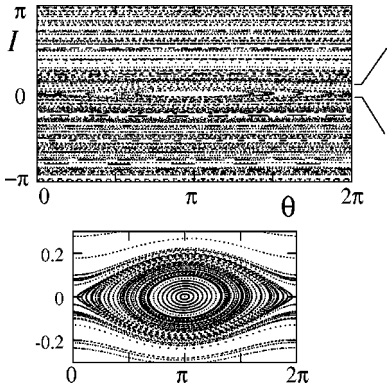

FIG. 6. Classical phase space for $k=0.01$. The lower figure zooms in on the region near $I=0$.

The classical phase space holds the key to understanding this: at $I_i=0$, almost all of the classical trajectories lie on small islets of stability as in the small oscillations of a pendulum (see Fig. 6). These islets have area smaller than $h/2$: approximating them as ellipses and calculating the maximum excursion in momentum to be $2\Delta k$ (from the approximate zeroth-order Hamiltonian $H_0=I^2/2+k\cos\theta$), gives the phase-space area of the largest islet as $\approx 0.6(h/2)$. Such islets do not exist quantum mechanically. Yet, the semiclassics is based on classical trajectories that lie on these quantum-mechanically invisible islets, and this is why the semiclassics fails: the semiclassical contributions differ in action by an amount much smaller than h.

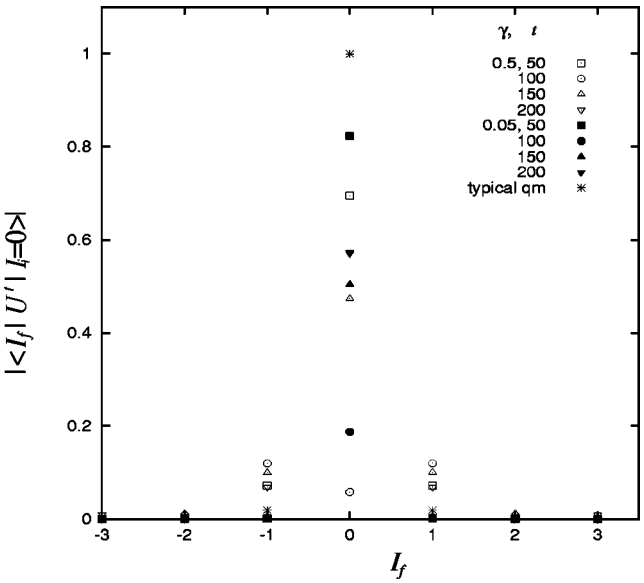

FIG. 5. $|\langle I_f|U^t|I_i=0\rangle|$ for $k=0.01$ at the times and values of γ indicated. The * indicates the typical quantum amplitude that hardly changes as time evolves (see the text).

We note that this is quite different from the situation of fine phase-space structure in chaotic systems,[19] which is further discussed in the next section. There (and also in the next section), the classical phase space has structures very fine on the scale of Planck's constant that have arisen from the classical manifold making large excursions in phase space and folding back near itself so is quite different from the present sub-h structure. Semiclassics works well there because, in contrast to the present section, typical contributions have action differences much larger than h.

The semiclassics depends on the value of the Gaussian width parameter. Unlike the previous section, there is no value of γ for which the sub-h problem goes away: for any γ, a significant fraction of the coherent state overlaps with sub-h islets. The semiclassics based on different γ is different, as shown in the figures. Consider Fig. 5. The quantum amplitude stays very near 1 at $I_i=0$ and almost 0 elsewhere always (the deviations being due to classically forbidden leakage). That the $\gamma=0.5$ case has considerable transport to states $I_f=I_i\pm 1$ can be understood from considering that the momentum width of the coherent states in the expansion is $\Delta I=\hbar\sqrt{\gamma}\approx 0.7$: because of the sub-$h$ islets, the semiclassical terms are being added with the incorrect phases determined by the classical trajectories and do not cancel out where they ought to. A representation with smaller momentum width, such as for $\gamma=0.05$ does not have the problem of amplitude on states $I_f\neq I_i$, since no classical trajectories ever reach these momenta. But, as for any γ, it still gets an incorrect magnitude on $I_f=I_i$. This brings to mind the work on atom–diatom scattering,[18] where the elastic transition was hard to get right when transitions to all other states are highly forbidden.

As k increases somewhat, so does the size of the islets and the expectation is that the semiclassical approximation gets better here: since a smaller fraction of the classical trajectories lie on islets of the sub-h area. This is confirmed in Fig. 7, where we have plotted Δ for three different values of k. The plot uses the semiclassics without renormalizing;

Downloaded 06 Jun 2003 to 128.6.71.61. Redistribution subject to AIP license or copyright, see http://ojps.aip.org/jcpo/jcpcr.jsp

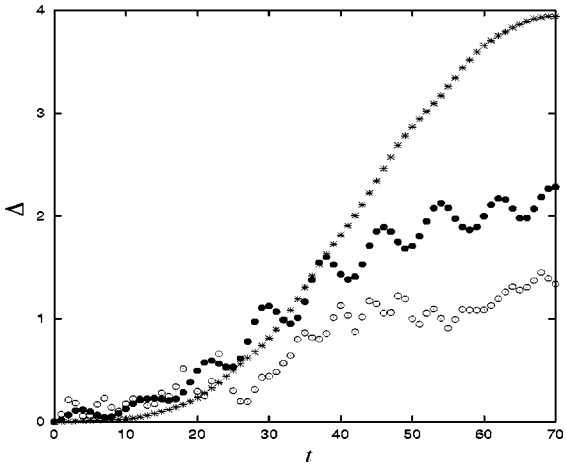

FIG. 7. Δ for $k=0.1$ (*), 0.5 (●), and 1.0 (○), as a function of time, where the initial state is $|I_i=0\rangle$.

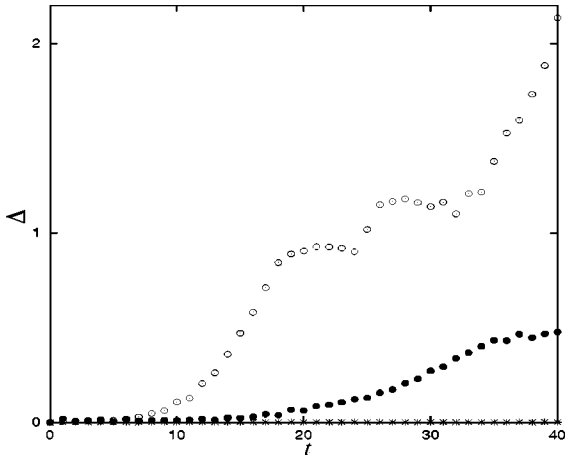

FIG. 9. $\triangle$ for $k=0.1$ (*), 0.5 (●) and 1.0 (○) as a function of time, where the initial state is $|I_i=3\rangle$.

when renormalized the result is similar but, in fact, a little worse.

We notice oscillations at $k=0.5$ that are also present in the norm plotted in Fig. 8. These have period corresponding to the inverse frequency of small oscillations in the sub-h islets. The latter can be calculated by a harmonic approximation to the small oscillations of the pendulum Hamiltonian above:

$$T=2\pi/\omega=2\pi/\sqrt{k}$$

For $k=0.5$, this gives $T\approx 8.8$, which agrees with the period of oscillations in the plots. This signature of the islets confirms our belief that the poorness of the semiclassics is due to sub-h islets. The oscillations are due to the interference of their contributions: periodically, the error in the amplitude decreases and increases as their contributions partially cancel and add, respectively. The harmonic oscillations do not appear clearly at all values of k and $\hbar$: they appear only when a significant fraction of the sub-h islets are truly harmonic. For example, for $k=0.1$, they do not appear for $\hbar=1$ (Fig. 7), but they are certainly present at $\hbar=0.5$, and they have a period around 20, consistent with the above.

For smaller $\hbar$, since there are fewer islets that have area less than $h/2$, we expect the semiclassical approximation to be better. Indeed this is true, as shown in Fig. 8 for $k=0.5$, for example.

Finally, in Fig. 9 we plot Δ for an initial state at $I_i=3$ and notice that this follows the opposite trend as a function of k as for $I_i=0$: for very small k, the semiclassics is excellent but gets worse for larger k. The phase space $I_i=3$ is essentially free-rotorlike at very small k, much like the unperturbed case. As k is turned up, the phase space acquires more structure (see Fig. 1), breaking up into periodic orbit chains and small zones of chaos and also invariant tori and cantori. So the initial state overlaps more sub-h structure as k increases.

As k continues to increase, these structures disintegrate as the phase space becomes more chaotic, and we expect that past a certain k, the semiclassics should again work well, in principle. There are inaccuracies from sub-h areas near possible caustics close to the real phase plane from the ever-increasing number of folds in the manifold, but the idea is that these are dominated by the ''good'' contributions that have large excursions in action.[19] We encounter, however, another problem in that regime: the highly oscillatory integral becomes increasingly difficult to converge. Unlike this section and the previous one, this problem is a practical problem rather than a fundamental one. We will discuss large k in the next section.

Note that the sub-h structure is not a problem for the special case of a harmonic system due to the property that all the islets, including those of area less than Planck's constant, have the same frequency, so in a sense are dynamically equivalent and correct. When the action is quadratic the stationary phase value of the integral leading to the semiclassical expression is always exact.

One implication of the results in this section is that semiclassical methods cannot be expected to work well near, for example, the critical parameter for the onset of global chaos

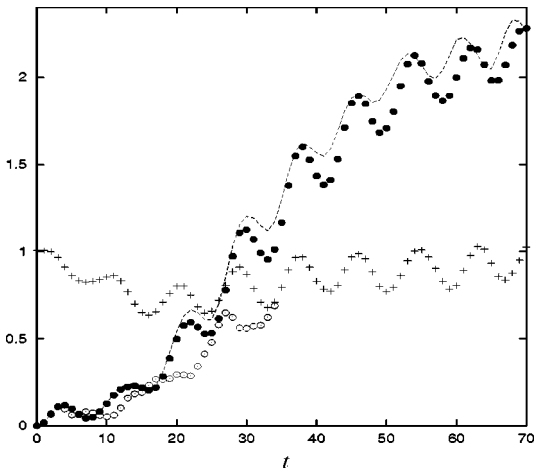

FIG. 8. $k=0.5$: the semiclassical norm (+), the error $\triangle$ (●), $\triangle$ for the renormalized semiclassics (dashed line), and $\triangle$ for $\hbar=0.5$ (⊙).

Downloaded 06 Jun 2003 to 128.6.71.61. Redistribution subject to AIP license or copyright, see http://ojps.aip.org/jcpo/jcpcr.jsp

where the classical phase space has intricate structures such as small islets nested around cantori. In fact, we expect semiclassics will not give a good description of motion after intermediate times close to the separatrices in generic near-integrable systems because of this.

V. CHAOTIC REGIME AND DYNAMICAL LOCALIZATION

In this section we look at a larger value of k for which the standard map is globally chaotic. Our aim is to investigate how good our semiclassical propagator (2.10) is in chaotic phase spaces. As pointed out a few years ago,[19] chaos is not an impediment to the validity of semiclassics, and we shall discuss this further shortly. In particular, we wish to investigate whether our semiclassics can predict dynamical localization: this is when the classical momentum diffuses but the quantum momentum is localized due to interference. The quantum behavior is in striking contrast to the classical.

Dynamical localization was discovered in the 1980s,[13] where the kicked rotor at large k was studied, and, in contrast to the classical behavior, the energy was found to be bounded at long times. The energy and momentum become quasiperiodic in time. In the classical kicked rotor the angle undergoes fast, quasirandom jumps while the momentum slowly diffuses out without bound $\langle \Delta I^2(t) \rangle = Dt$. At short times the quantum system follows classical diffusive behavior. But before $\langle \Delta I^2 \rangle$ gets ''too big,'' quantum interference between classical paths becomes important and the system begins to localize. In the quantum dynamics, $\langle \Delta I^2 \rangle$ stops growing and undergoes quasiperiodic behavior in time. In a sense, there is nothing new in the quantum mechanics after this ''break time,'' or quantization time, which is the inverse level spacing: the system has resolved the finite spectrum and already explored all of the eigenstates in the initial wave packet. When the classical diffusion is linear in time with diffusion constant D, as it is for sufficiently chaotic classical systems, it is not difficult to show that the localization length in momentum l_I is $l_I \equiv \sqrt{\Delta I^2}|_* \propto D/\hbar = k^2/2\hbar$ and that the break time is $t_b \approx l_I \approx k^2/2\hbar$. The $|_*$ indicates the localized value and we have, in the last step, put in the diffusion constant for the kicked rotor at large k. Eigenstates of the map are exponentially localized and l_I also gives (up to a factor) the decay factor.

There is a deep connection between dynamical localization and Anderson localization: one can map the kicked rotor onto the problem of a quantum particle in a one-dimensional lattice with random impurities.[13] In the lattice problem, if the site energies are randomly chosen from some fixed distribution then it can be proven that all electron eigenstates are exponentially localized around a lattice site, and this effect is called Anderson localization. The quantum transport vanishes and the quantum particle undergoes quasiperiodic motion. In chaotic systems such as the kicked rotor, there is no randomness in the Hamiltonian, rather the randomness emerges out of the dynamics; hence the term ''dynamical localization.''

Dynamical localization occurs in many atomic and molecular systems.[9] Perhaps the most well-studied example is that of Rydberg atoms in microwave fields. This is a member of a class of periodically driven nonlinear oscillators, where $H = H_0(I) + \epsilon x \sin(\omega t)$, in which dynamical localization can occur. For example, if $H_0(I)$ is the Morse Hamiltonian, this can represent multiphoton absorption by molecular vibrations and dynamical localization can suppress the extent of the resulting ionization and dissociation. Other examples include periodically driven Josephson junctions that can be modeled by a periodically driven pendulum; the latter also models many quantum optical systems, for example, the deflection of an atomic beam passing a standing wave laser field in front of a vibrating mirror. We refer the reader to the literature and references therein.

It is supposed that quantum interference is enough to explain dynamical localization. Since semiclassics has interference built into it, we expect that semiclassics should be able to reproduce this effect. This has been very difficult to test because of the chaos: for example, in the boundary-value formulation, the exponential proliferation of classical paths as time evolves makes the semiclassical sum almost impossible to compute. Progress has been made recently,[14] where an iterated version of semiclassics in a boundary-value representation was considered for a particularly designed map that has no caustics in that representation. The semiclassics for a time T was computed and longer times were obtained by iteration. Assuming larger and larger T converges to the true long-time semiclassics, semiclassical dynamical localization was demonstrated.

In this section, we attempt to show semiclassical dynamical localization directly for the kicked rotor, using the initial-value representation semiclassical propagator (2.10).

How well does semiclassics cope in a chaotic phase space? In the early 1990s,[19] semiclassics was shown to be remarkably accurate in the stadium billiard: although there is an intricate structure in the chaotic classical phase space on scales much finer than h, these classical trajectories are well separated in action. Due to the chaos in our map at large k, we expect that most neighboring trajectories make large excursions in phase space, so that contributions to the semiclassical sum enclose areas far greater than h. This suggests that for the chaotic limit of our map, semiclassics should be a good approximation in principle, unlike in the previous section. However, here we have to deal with a different kind of semiclassical devil: the practical computation of the semiclassical propagator in the chaotic regime, as we mentioned above. In an initial-value formulation, such as the propagator (2.10), this translates into a highly oscillatory and exponentially increasing integrand: dynamical quantities are highly sensitive to initial conditions and, consequently, so is the phase of the integrand. The monodromy matrix elements contained in the prefactor, which measure the divergence of nearby trajectories, are exponentially increasing. This problem arises generically when applying semiclassics to complex systems and the number of trajectories required to converge the integrand often becomes prohibitively large. Much of the current research effort in semiclassics is in how to handle this problem.[6] Unlike the devils in the previous sections, however, this devil is not a devil in principle. To a certain degree it can be tamed by using smoothing techniques[20–22] that have been developed for this purpose. In

Downloaded 06 Jun 2003 to 128.6.71.61. Redistribution subject to AIP license or copyright, see http://ojps.aip.org/jcpo/jcpcr.jsp

particular, we shall use a smoothing based on ''cellular dynamics.'' [21]

Cellular dynamics smoothing is based on linearization in small cells, and has been shown to work effectively in a number of situations,[22,23] obtaining good convergence for semiclassical amplitudes with fewer trajectories than would otherwise be needed. In particular,[22] it has been used on the Herman–Kluk propagator between coherent states to find Franck–Condon factors. The case here is very similar. We insert the identities $\sqrt{\alpha/\pi}\Sigma_m\int_0^{2\pi} d\theta' \exp[-\alpha(\theta'+2\pi m-\theta_0)^2]=1$ and $\sqrt{\beta/\pi}\int_{-\infty}^{\infty} dI' \exp[-\beta(I'-I_0)^2]=1$ into Eq. (2.10). The order of integration is switched and α, β are considered large validating low-order expansions of functions of (θ_0',I_0') in the integrand around (θ_0,I_0) (linearizations). The integral over (θ_0,I_0) becomes Gaussian and thus able to be performed easily. The result for the smoothed propagator then becomes

$$\langle I_f|U^n|I_i\rangle=\frac{\sqrt{\alpha\beta}}{2\pi\hbar}\int_0^{2\pi} d\theta_0\int_{-\infty}^{\infty} dI_0\langle I_f|\theta_n,I_n\rangle \times\frac{C_{\theta_0,I_0,n}}{\sqrt{\det A}}e^{b^TA^{-1}b/4}e^{iF(\theta_0,I_0,n)/\hbar}\langle\theta_0,I_0|I_i\rangle, \tag{5.1}$$

where

$$b=\begin{pmatrix} \dfrac{i(I_o-I_i)}{\hbar}+\left(\dfrac{1}{2\hbar^2\gamma}\dfrac{\partial I_n}{\partial\theta_0}-\dfrac{i}{\hbar}\dfrac{\partial\theta_n}{\partial\theta_0}\right)(I_n-I_f) \\ \dfrac{I_o-I_i}{2\hbar^2\gamma}+\left(\dfrac{1}{2\hbar^2\gamma}\dfrac{\partial I_n}{\partial I_0}-\dfrac{i}{\hbar}\dfrac{\partial\theta_n}{\partial I_0}\right)(I_n-I_f)\end{pmatrix} \tag{5.2}$$

and

$$A=\begin{pmatrix} \alpha+\dfrac{1}{4\hbar^2\gamma}\left(\dfrac{\partial I_n}{\partial\theta_0}\right)^2-\dfrac{i}{2\hbar}\dfrac{\partial I_n}{\partial\theta_0}\dfrac{\partial\theta_n}{\partial\theta_0} & \dfrac{1}{4\hbar^2\gamma}\dfrac{\partial I_n}{\partial\theta_0}\dfrac{\partial I_n}{\partial I_0}-\dfrac{i}{2\hbar}\dfrac{\partial I_n}{\partial\theta_0}\dfrac{\partial\theta_n}{\partial I_0} \\ \dfrac{1}{4\hbar^2\gamma}\dfrac{\partial I_n}{\partial\theta_0}\dfrac{\partial I_n}{\partial I_0}-\dfrac{i}{2\hbar}\dfrac{\partial I_n}{\partial\theta_0}\dfrac{\partial\theta_n}{\partial I_0} & \beta+\dfrac{1}{4\hbar^2\gamma}+\left(\dfrac{\partial I_n}{\partial I_0}\right)^2-\dfrac{i}{2\hbar}\dfrac{\partial I_n}{\partial I_0}\dfrac{\partial\theta_n}{\partial I_0}\end{pmatrix}. \tag{5.3}$$

If α and β are chosen large enough, the real part of $\det A$ is ensured to remain positive throughout the period and no correction is needed for the choice of branch of its square root.

As time evolves and the manifolds become increasingly convoluted, the cell size for which the linearization is valid shrinks and larger and larger values of the smoothing parameters α and β are needed. We ensure that our results are converging to the true (infinite α, β limit) by testing invariance with respect to these large parameters and convergence with the number of trajectories.

We shall take $k=4$, which is not very large, but large enough that the classical dynamics exhibits momentum diffusion and quantum dynamical localization. We begin our initial state at $I_i=3$, which lies in a chaotic zone for this value of k (see Fig. 1), and we choose the unbiased value of $\gamma=0.5$ for the width of the coherent states in (2.10). The integration is performed as a sum on a grid that is evenly spaced in θ and the positions of the I abscissas are determined by the weighting provided by the initial state (more densely spaced near I_i and exponentially less densely farther out).

The magnitude of the quantum and semiclassical transition probabilities at certain times are plotted in Fig. 10. For the largest times at which we have achieved convergence, the smallest value of the smoothing parameters that give the true semiclassics is $\alpha=\beta=10^{16}$. We check that using 10^{17} does not alter the result. The value of the valid smoothing parameter grows with time since nonlinearity develops on smaller and smaller scales. The number of trajectories needed grows exponentially as a function of time as the extent of folding of the manifold does: to get an accurate and converged semiclassical amplitude, one needs to sample each fold by at least a few trajectories. For the largest time we used 4.7×10^8 trajectories. We note here an advantage of the discrete-time map: to propagate this number of trajectories up to the corresponding physical time in continuous time would take much more computational time.

The norm of the wave function as a function of time is plotted in Fig. 11. We observe that the semiclassics becomes increasingly nonunitary as time goes on. This suggests that even the renormalized semiclassical approximation becomes worse at longer times: this is supported by the inset, which plots Δ for the renormalized semiclassics.

In Fig. 12 we have plotted the momentum dispersion $(\Delta I)^2=\langle(I-I_i)^2\rangle$, where $I_i=3$ (the initial momentum) as time evolves. The classical diffusion constant is about 6.5 for this case, measured after the initial transients (which is close to the theoretical value of $k^2/2=8$ valid for larger k). The quantum points follow the classical roughly until about $t=8$, when the quantum curve begins to keel over. For much longer times it oscillates around about 60. $t=8$ is the break time, and is consistent with the theoretical value. The renormalized semiclassical dispersion follows the quantum and classical roughly until this time and then begins to localize, although somewhat differently from the quantum localization. We suspect that the discrepancies arise mostly from inaccuracies due to caustics near the real phase plane, and also hard quantum effects such as tunneling. In our semiclassical formulation, although there are never any caustics for real trajectories, there can be inaccuracies generated from caustics nearby in the complex phase plane, from the exponentially increasing folding of the manifold. Unfortunately,

Downloaded 06 Jun 2003 to 128.6.71.61. Redistribution subject to AIP license or copyright, see http://ojps.aip.org/jcpo/jcpcr.jsp

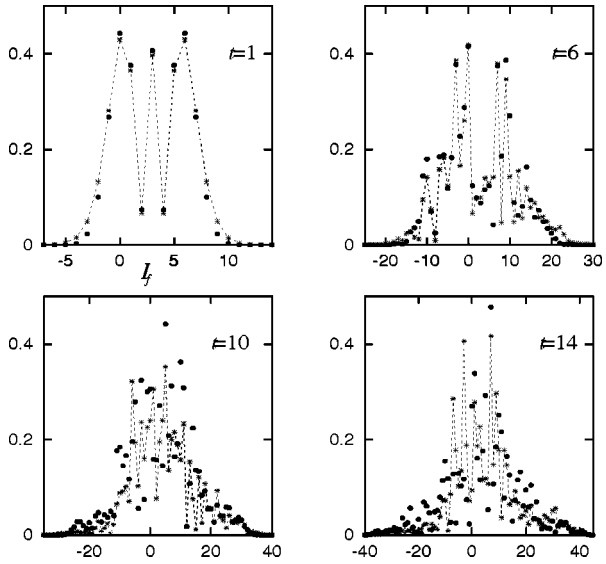

FIG. 10. $|\langle I_f|U^n|I_i=3\rangle|$ at the times indicated for $k=4$. The quantum is * connected by dashed lines for ease of visualization, and the semiclassical is ●.

the calculation time (number of trajectories) becomes too long to achieve convergence for longer times. We suspect the semiclassical approximation gets worse and becomes increasingly nonunitary, however, it would still be interesting to see if it continues to localize.

In the recent study[14] described briefly at the beginning of this section, semiclassical localization was observed, and, as in our case, the details were different from the quantum; there the differences were attributed to diffraction and tunneling corrections.

Our results imply that dynamical localization is largely due to interference and not some other quantum effect. In fact, we can check this more directly by comparing the average slopes of the dispersion lines of the semiclassical integral and an integral of the same form as (2.10), but with all the phases taken out (including phases in the coherent state projections and prefactor), i.e., we integrate the *magnitude* of the integrand. After renormalizing, this is plotted as the open

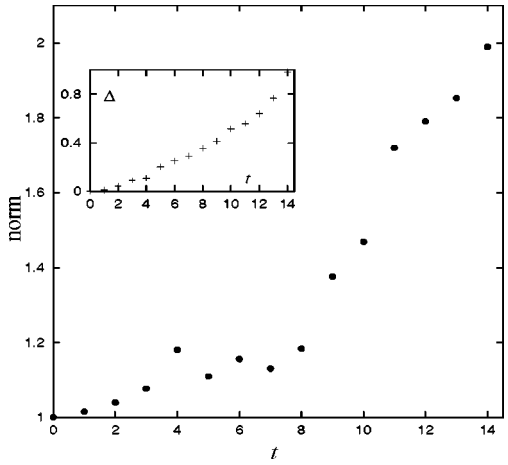

FIG. 11. The norm of the semiclassical wave function, $\Sigma_j|\langle I_j|U^n|I_i=3\rangle|^2$ (for $k=4$). The inset shows $\triangle$ using the renormalized semiclassics.

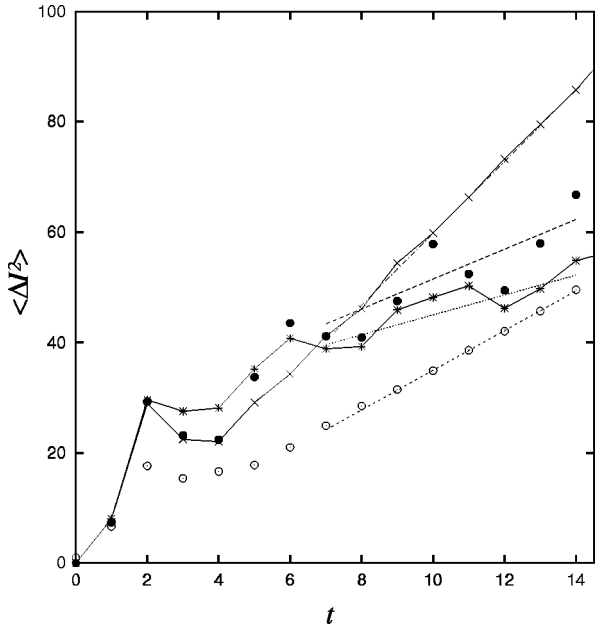

FIG. 12. The momentum diffusion, $\langle(\Delta I)^2\rangle$, for $k=4$ and $I_i=3$. The graphs are classical ($-\times-$) quantum ($-*-$), semiclassical (●), and the semiclassical integral without phases (⊙). The lines are fits to the average dispersion measure after the break time (see the text): the dashed–dotted line (fit for classical) has slope 6.5, the dotted line (fit for quantum) has slope 1.9, the long-dashed line (fit for semiclassical) has slope 2.7, and the short-dashed line (fit for semiclassics with the phases neglected) has slope 3.6.

circles in Fig. 12. Note that only in the limit that $h\to 0$ does this reduce to the classical quantity. In that limit the integral (2.10), including phases, reduces to its stationary phase value, which is equal to the boundary-value formula (2.1). If we take the phases out of this latter formula, we would get the classical result; this is not true for the initial value formulation (2.10), which is distinct from the boundary-value form (except in the limit that $\hbar\to 0$) due to the integration over initial phase space being done exactly numerically rather than by the stationary phase. Like the classical, the slope of this line does not show any transition at the break time, which is in contrast to the quantum and true semiclassical: the latter both have a steeper slope (classical-like diffusion) before the break time, where the localization begins to set in. This indicates that the semiclassical localization is due to phase interference. The slope of the line that fits the quantity obtained from the semiclassics without phases, measured after the initial transients, is 3.6. The average slope of the true semiclassics and the quantum, measured between the break time and time 14, are around 2.7 and 1.9, respectively.

VI. CONCLUSIONS

In this paper we have presented and studied a semiclassical propagator in initial-value representation for a discrete-time map on a cylinder. Discrete-time maps are an efficient way to capture the dynamics of a continuous-time system. In this paper we continue the trend in the recent literature[3,4] toward exploring this by investigating semiclassics in such a setting. Our semiclassical propagator is adapted from Herman and Kluk's.[8]

Downloaded 06 Jun 2003 to 128.6.71.61. Redistribution subject to AIP license or copyright, see http://ojps.aip.org/jcpo/jcpcr.jsp

We have shown that our semiclassical propagator can provide a good approximation of the quantum dynamics in many situations, and, in situations where it is not good, we have shown why. We have studied the kicked rotor, which, although a one-dimensional system, displays great complexity of behavior and phenomena, which are present in generic high-dimensional molecular systems: our model is thus also a test of how well the propagator, and semiclassical methods, in general, can describe such phenomena.

We investigated classically forbidden transport in studying the transitions to states not reached by the classical distribution in one iteration. Our results confirm some similar conclusions in recent work[11,12] regarding the relevance of branch cuts in the complex plane in the semiclassical description of tunneling. In general, these hide the complex stationary phase points behind them. In a Herman–Kluk propagator, there is a free parameter γ that can be tuned so to push the branch cuts away beyond the stationary phase point. Only then can the real trajectories of the semiclassical propagator describe classically forbidden processes accurately. We performed this explicitly for one iteration of our map. Of course, for a general situation, finding the right parameter to do this is very difficult, and generically, the parameter will itself be complex.[11] The success of real trajectories to describe classically forbidden processes, in principle, relies on an integration through real trajectories being deformable to one through the complex stationary phase point. Here there was a parameter in the problem that can be chosen at will to achieve this, but this is not always the case.[12] This was discussed in Sec. III.

We studied the effect of islets of stability of area below the size of Planck's constant on the semiclassical propagator in Sec. IV. This can lead to inaccuracies in the semiclassics: Quantum mechanics smears the structure, yet semiclassics is based on classical trajectories whose dynamics is determined by them. We first encountered a somewhat benign case of this in Sec. III: when a caustic in the complex plane is very close to the real axis. There, effectively changing the representation in which the semiclassics is done cures the problem. In Sec. IV, we discussed a situation where semiclassics in any representation fails: this is in the presence of sub-h islets of stability.

Finally, in Sec. V we considered the phenomenon of dynamical localization that occurs in the chaotic limit of our map. The classical momentum diffuses without bound while the quantum, in contrast, localizes after an initial diffusion. We showed that the semiclassics also begins to localize, and we confirmed that this is due to phase interference between the classical trajectories by considering the semiclassical integrand neglecting the phases. The semiclassical localization does not track the quantum exactly and seems weaker, when one compares the average slope of the two after the break time. Moreover, the semiclassics becomes increasingly nonunitary. We suspect that the discrepancies are due to nearby caustics in the complex plane and tunneling corrections. We note that a recent study[14] showed this effect for a certain caustic-free map using an iterated semiclassics, as described in the previous section. In this paper we have demonstrated semiclassical dynamical localization for the kicked rotor directly using semiclassics in an initial-value representation. We are able to propagate long enough to see the semiclassical localization begin to set in but cannot carry out the computation for very much longer because of the exponentially increasing number of trajectories needed to converge the semiclassical integral as time goes on.

ACKNOWLEDGMENTS

The author is very grateful to Bill Miller for many inspiring discussions on semiclassics and valuable suggestions regarding the manuscript. She would also like to thank Michael Thoss and Haobin Wang for fruitful conversations, Chris Woodward for a useful suggestion regarding the numerical integration, and the referee for helpful comments. This work has been supported by the National Science Foundation under Grant No. CHE 97-32758.

[1] H. Poincaré, *Les Methods Nouvelles de la Mechanique Celeste* (Gauthier-Villars, Paris, 1892); A. J. Lichtenberg and M. A. Lieberman, *Regular and Chaotic Dynamics* (Springer-Verlag, New York, 1983); M. Tabor, *Chaos and Integrability in Non-Linear Dynamics, an Introduction* (Wiley, New York, 1989).
[2] B. V. Chirikov, Phys. Rep. **52**, 263 (1979); J. M. Greene, J. Math. Phys. **20**, 1183 (1979).
[3] E. Rabani and B. J. Berne, J. Phys. Chem. A **102**, 9380 (1998); E. Rabani and R. D. Levine, J. Chem. Phys. **104**, 1937 (1996); M. E. Tuckerman, G. J. Martyna, and B. J. Berne, *ibid.* **93**, 1287 (1990).
[4] S. S. Abdullaev, J. Phys. A **32**, 2745 (1999).
[5] V. P. Maslov and M. V. Fedoriuk, *Semiclassical Approximations in Quantum Mechanics* (Reidel, Dordrecht, 1981); J. H. Van Vleck, Proc. Natl. Acad. Sci. USA **14**, 178 (1928); M. C. Gutzwiller, J. Math. Phys. **8**, 1979 (1967); R. Balian and C. Bloch, Ann. Phys. (N.Y.) **69**, 76 (1972); M. V. Berry and K. E. Mount, Rep. Prog. Phys. **35**, 315 (1972); W. H. Miller, Adv. Chem. Phys. **25**, 69 (1974); E. J. Heller, in *Lectures in 1989 NATO Les Houches lectures, Summer School on Chaos and Quantum Physics*, edited by M-J. Giannoni, A. Voros, and J. Zinn-Justin (Elsevier, Amsterdam, 1991), p. 547.
[6] W. H. Miller, Faraday Discuss. **110**, 1 (1998), and references therein.
[7] E. J. Heller, J. Chem. Phys. **94**, 2723 (1991); W. H. Miller, *ibid.* **53**, 1949 (1970); **53**, 3578 (1970); W. H. Miller, *ibid.* **95**, 9428 (1991); E. J. Heller, *ibid.* **95**, 9431 (1991).
[8] M. F. Herman and E. Kluk, Chem. Phys. **91**, 27 (1984); E. Kluk, M. F. Herman, and H. L. Davis, J. Chem. Phys. **84**, 326 (1986); K. G. Kay, *ibid.* **100**, 4377 (1994).
[9] G. Casati, I. Guarneri, and D. L. Shepelynaski, IEEE J. Quantum Electron. **QE 24**, 1420 (1988); R. Blumel and U. Smilansky, Phys. Rev. Lett. **52**, 137 (1984); Phys. Rev. A **30**, 1040 (1984); R. Graham and M. Hohnerbach, Phys. Rev. Lett. **64**, 637 (1990); R. Graham, M. Schlautmann, and D. L. Shepelyansky, *ibid.* **67**, 255 (1991); R. Graham, M. Schlautmann, and P. Zoller, Phys. Rev. A **45**, R19 (1992).
[10] S. Keshavamurthy and W. H. Miller, Chem. Phys. Lett. **218**, 189 (1994); B. Spath and W. H. Miller, J. Chem. Phys. **104**, 95 (1996).
[11] K. G. Kay, J. Chem. Phys. **107**, 2313 (1997).
[12] F. Grossmann and E. J. Heller, Chem. Phys. Lett. **241**, 45 (1995); N. T. Maitra and E. J. Heller, Phys. Rev. Lett. **78**, 3035 (1997); N. T. Maitra and E. J. Heller, *Classical, Semiclassical and Quantum Dynamics in Atoms*, Springer Lecture Notes in Physics, edited by H. Friedrich and B. Eckhardt (Springer-Verlag, Berlin, 1997).
[13] G. Casati, B. V. Chirikov, F. M. Izrailev, and J. Ford in *Stochastic Behavior in Classical and Quantum Hamiltonian Systems*, Vol. 93 of Lecture Notes in Physics, edited by G. Casati and J. Ford (Springer-Verlag, Berlin, 1979); B. V. Chirikov, F. M. Izrailev and D. L. Shepelyansky, Sov. Sci. Rev., Sect. A **2**, 209 (1981); T. Hogg and B. A. Huberman, Phys. Rev. Lett. **48**, 711 (1982); F. Haake, *Quantum Signatures of Chaos* (Springer-Verlag, Berlin, 1991); D. R. Grempel, R. E. Prange, and S. Fishman, Phys.

Downloaded 06 Jun 2003 to 128.6.71.61. Redistribution subject to AIP license or copyright, see http://ojps.aip.org/jcpo/jcpcr.jsp

Rev. A **29**, 1639 (1984); P. W. Anderson, Phys. Rev. Lett. **109**, 1492 (1958); P. W. Anderson, Rev. Mod. Phys. **50**, 191 (1978).
[14] L. Kaplan, Phys. Rev. Lett. **81**, 3371 (1998).
[15] H. Goldstein, *Classical Mechanics*, 2nd ed. (Addison-Wesley, Reading, MA, 1980).
[16] E. J. Heller, J. Chem. Phys. **75**, 2923 (1981); **62**, 1544 (1975); **65**, 4979 (1976).
[17] F. Grossmann and A. L. Xavier, Jr., Phys. Lett. A **243**, 243 (1998); Y. Weissman, J. Phys. A **16**, 2693 (1983).
[18] W. H. Miller, Adv. Chem. Phys. **30**, 77 (1975); J. Chem. Phys. **53**, 3578 (1970); Chem. Phys. Lett. **7**, 431 (1970).
[19] S. Tomsovic and E. J. Heller, Phys. Rev. Lett. **67**, 664 (1991); M. A. Sepúlveda, S. Tomsovic, and E. J. Heller, *ibid.* **69**, 402 (1992); S. Tomsovic and E. J. Heller, Phys. Rev. E **47**, 282 (1993).
[20] V. S. Filinov, Nucl. Phys. B **271**, 717 (1986); N. Makri and W. H. Miller, Chem. Phys. Lett. **139**, 10 (1987); J. D. Doll, D. L. Freeman, and T. L. Beck, Adv. Chem. Phys. **78**, 61 (1994); B. E. Guerin and M. F. Herman, Chem. Phys. Lett. **286**, 361 (1998).
[21] E. J. Heller, J. Chem. Phys. **94**, 2723 (1991).
[22] A. R. Walton and D. E. Manolopoulos, Mol. Phys. **87**, 961 (1996).
[23] M. A. Sepúlveda and E. J. Heller, J. Chem. Phys. **101**, 8004 (1994); **101**, 8016 (1994); M. L. Brewer, J. S. Hulme, and D. E. Manolopoulos, *ibid.* **106**, 4832 (1997).

Downloaded 06 Jun 2003 to 128.6.71.61. Redistribution subject to AIP license or copyright, see http://ojps.aip.org/jcpo/jcpcr.jsp